Heliyon 10 (2024) e31767

Contents lists available at ScienceDirect

Heliyon

journal homepage: www.cell.com/heliyon

Research article

Nonlinear robust sliding mode - Backstepping hybrid control for WECS -theoretical design and experimental evaluation

Farah Echiheb [a,b], Ismail Elkafazi [b], Badre Bossoufi [a,*], Brahim El bhiri [b], Mishari Metab Almalki [c], Thamer A.H.Alghamdi [d,e,**]

[a] LIMAS Laboratory, Faculty of Sciences Dhar El Mahraz, Sidi Mohammed Ben Abdellah University Fez, Morocco
[b] SMARTilab Laboratory, Moroccan School of Engineering Sciences Rabat, Morocco
[c] Department of Electrical Engineering, College of Engineering, Al-Baha University, Al Aqiq, Saudi Arabia
[d] Wolfson Centre for Magnetics, School of Engineering, Cardiff University, Cardiff, CF24 3AA, UK
[e] Electrical Engineering Department, School of Engineering, Al-Baha University, Al-Baha, 65779, Saudi Arabia

ARTICLE INFO

Keywords:
Doubly fed induction generator DFIG
Maximum power point tracking MPPT
Field oriented control FOC
Sliding mode control SMC
Rotor side converter RSC
Grid side converter GSC
Backstepping control BS

ABSTRACT

This paper proposes a new contribution in the field of optimizing control techniques for wind systems to enhance the quality of the energy produced in the grid. Although the Sliding Mode control technique, whether classical or involving the use of artificial intelligence, has shown interesting results, its main drawback lies in the oscillation phenomenon commonly referred to as "chattering." This phenomenon affects the accuracy and robustness of the system, as well as the parametric variation of the system. In this work, we propose a solution that combines two nonlinear techniques based on the Lyapunov theorem to eliminate the chattering phenomenon. It is a hybrid approach between the Backstepping strategy and the Sliding Mode, aiming to control the active and reactive powers of the doubly fed induction generator (DFIG) connected to the electrical grid by two converters (grid side and machine side). This hybrid technique aims to improve the performance of the wind system in terms of precision errors, stability, as well as active and reactive power. The proposed solution has been validated in the Matlab & Simulink environment to assess the performance and robustness of the proposed model, as well as experimentally validated on a test bench using the DSPACE 1104 card. The obtained results are then compared with other techniques, demonstrating a significant improvement in performance.

V	Wind speed (m/s)	C_{t-est}	Estimated torque of the turbine
P_{aero}	Aerodynamique power	M	Cyclic mutual inductance between stator and rotor
P_{mec}	Mechanical power	C_{em}	Electromagnetic torque
R,	Radius of the turbine, Gearbox gain	C_{aero}	Aerodynamic torque
f_s, f_r	Stator and Rotor frequency	f	Coefficient of viscous friction
P_s, P_r	Stator and Rotor active power	J_{tot}, J_t, J_g	Total inertia, Turbine inertia and inertia of generator
Q_S, Q_r	Stator and Rotor reactive power	$\varphi_{s,rd}, \varphi_{s,rq}$	Stator and Rotor Flux in plane d – q d-q
P_c	Active power at the capacitor	$v_{s,rd}, v_{s,rq}$	Stator and Rotor Voltage in plane d – q

(*continued on next page*)

* Corresponding author.
** Corresponding author. Wolfson Centre for Magnetics, School of Engineering, Cardiff University, Cardiff, CF24 3AA, UK.
E-mail addresses: badre.bossoufi@usmba.ac.ma (B. Bossoufi), Alghamdit1@cardiff.ac.uk (T. A.H.Alghamdi).

https://doi.org/10.1016/j.heliyon.2024.e31767
Received 12 March 2024; Received in revised form 18 May 2024; Accepted 21 May 2024
Available online 22 May 2024

(*continued*)

Ω_s, Ω_r	Synchronisme speed and Rotor speed	v_{fd}, v_{fq}	Filter Voltage in plane d – q
Ω_t	Turbine speed Specific density of air	I_{sd}, I_{sq}	Stator Current in plane d – q
ω_s, ω_r	Pulsation at stator and rotor	I_{rd}, I_{rq}	Rotor Current in plane d – q
g	Sliding of asynchronous machine	I_{fd}, I_{fq}	Filter Current in plane d – q
p	Number of poles pairs	V_{dc}	DC-BUS voltage
R_s, R_r	Stator and Rotor resistance	$S_{s,abc}$	Switching states of inverter
L_s, L_r	Stator and Rotor inductance	P_f, P_r	Filter and rotor active power
R_f, L_f	Filter resistance, Filter inductance		
ω_g	Grid pulsation		

1. Introduction

1.1. Overview

In the ever-evolving story of global energy, the winds of change are pushing us towards a cleaner, more sustainable future [1]. As the world grapples with the urgent need to address climate change and reduce dependence on finite fossil fuels [2], renewable energy sources [3,4] have emerged as beacons of hope. Among these, wind power stands out, harnessing the kinetic force of the wind to generate electricity and redefining the energy landscape [5].

The temperature and pressure differences caused by the absorption of solar rays in the atmosphere ensure that wind energy is an indirect form of solar energy. The movement of air masses accumulates kinetic energy, which can be transformed and used for a number of purposes, including the production of electrical energy. Three factors affect how much electricity a wind turbine can generate: the size and design of the blades, the wind speed, and the air density due to temperature. The amount of energy that can be recovered by a wind turbine depends on the area that its rotor sweeps and the cube of the wind speed [6].

Wind power, a form of renewable energy with ancient roots in sail-driven ships, has undergone a remarkable metamorphosis in recent decades. Today, it stands as a symbol of innovation and progress, contributing significantly to the diversification of our energy mix. Wind turbines, resembling modern-day giants with their towering blades, have become iconic symbols of sustainable energy production [7].

In the face of climate change and the imperative to reduce carbon emissions, countries worldwide are embracing wind power as a vital component of their energy portfolios [8]. International collaborations and agreements underscore the global commitment to transition towards sustainable practices, with wind power emerging as a key player in this collective effort [9]. Recent studies [10–12] have tried to prove that wind power is growing the fastest in the world in terms of development due to recent new renewable energy technology.

According to the European Parliament's Fact Sheets on the European Union [13], EU legislation on the promotion of renewable energies has evolved considerably over the last fifteen years. In 2018, EU leaders set a target of 32 % renewable energy in final energy consumption by 2030. In March 2023, in line with the EU's ambition to achieve climate neutrality by 2050, the co-legislators decided to increase the share of renewable energy to be achieved by 2030 to 42.5 %, with the hope of reaching 45 %. The updated Renewable Energy Policy Framework for 2030 and beyond is currently being negotiated.

In the present day, the realm of wind power is experiencing a surge in both technological advancements and global adoption [14]. The efficiency and capacity of wind turbines have soared to unprecedented heights, breaking barriers and setting new standards [15]. This surge is not confined to a single region; it's a global phenomenon that transcends borders. From wind-swept plains to coastal shores, wind farms are sprouting up, painting a hopeful picture of a planet transitioning towards cleaner, greener energy solutions.

Beyond environmental benefits [16], wind power is proving its economic mettle [17]. The falling costs of wind energy, coupled with governmental support and favorable policies, are making wind projects increasingly attractive. Furthermore, the industry is becoming a significant source of employment, breathing life into local economies through the construction, operation, and maintenance of wind farms [18].

The wind turbine is coupled to an electrical generator to create direct or alternating current [19]. Most generators used in wind turbines are three-phase asynchronous generators [20]. These have several advantages [21]: they are robust, low-cost and mechanically simple. The downside of the DFIG-based wind turbine is that it is extremely sensitive to load disturbances, variations in the turbine's rotational speed, and variations in the internal and external system parameters [22]. The system is similarly multi-variable, dynamic, tightly linked, and nonlinear, which makes controlling it very challenging. MPPT, which is the primary goal of the DFIG control system, is to efficiently capture wind energy, regardless of the weather [23,24].

Before delving into control strategies, it's essential to grasp the workings of the Doubly Fed Induction Generator. Known for its ability to control both the rotor and stator windings [25], DFIGs offer superior adaptability to varying wind conditions, making them indispensable in the quest for efficient and responsive wind power systems.

1.2. Literature review

Numerous studies in existing literature have aimed to develop a control system that is both effective and robust for both the RSC and the GSC of the wind power system's conversion chain to optimize energy production and ensure grid stability. Among these algorithms, linear control laws based on PI controllers have been explored [26], as well as controllers such as DPC or DTC [27], and

non-linear control laws such as SMC [28] and BSC [29].

PI controllers are commonly used in control systems to maintain the stability and performance of dynamic systems [30]. However, this does not preclude the existence of constraints that hinder the achievement of these objectives. The authors [31] apply IFOC based on traditional PI regulators to RSCs and GSCs. However, the major drawback of this control method is the high sensitivity of the control system to the parameters of the system under study and the need to adjust the coefficients of the PI controller. For [32], they propose the improved control method IFOC. This strategy controls the electrical parameters used to implement the regulation of the rotor current and electromagnetic torque components in a DFIG WECS. The disadvantage of this control is that the level of harmonic distortion of the rotor current remains, particularly in the case of low-voltage operating behaviour of the system, commonly known as voltage dips. In this context [33], propose a field-oriented control (FOC) of a rotor DFIG (RT-DFIG) using a high gain observer (HGO). But the observer-based control system may fail in case of current/voltage sensor failure which represents a limitation for HGO control.

Otherwise, in some cases, DPC or DTC controllers may be preferred over PI controllers for wind system control [34]. They offer improved control dynamics, enabling rapid adaptation to changing wind conditions and efficient optimization of energy production [35]. These controllers ensure a rapid response to disturbances, promoting wind system stability in the face of sudden changes in wind conditions or variations in the electrical grid. In addition, their ability to directly adjust electrical power or torque contributes to better power management, improving the efficiency of wind energy conversion [36]. They are also effective at reducing unwanted oscillations, improving the quality of the electricity generated and minimising the impact on the grid [37]. Because of their adaptability to varying conditions, these advanced controllers are well suited to adjusting quickly to changes, ensuring optimum performance in a dynamic wind environment [38]. As in the paper by Ref. [39], the authors considered that flux and torque estimation is the basis of DTC and power estimation is the basis of DPC to keep the bus voltage constant. Also, for the authors [40], they propose an improved control strategy to conventional DPC that limits oscillations under unbalanced grid voltage conditions. Unfortunately, the slow response and large ripples in active and reactive power remain a drawback for this control.

Linear controls often require the linearisation of models to make systems easier to manage. However, linearisation can lead to inaccurate approximations, especially when variations around the nominal operating point are large [41]. For this reason, researchers are turning to non-linear controls that eliminate the need for linearisation. Non-linear controls are often more flexible and adaptive to variations in system parameters [42]. They can handle situations where system parameters change, and are also capable of providing faster responses to changes in conditions or references.

Some non-linear approaches are based on Lyapunov theory, such as SMC [43] and BSC [44,45]. In the paper by Ref. [46], the authors apply a non-linear, super-twist and knock terminal sliding mode control system (ST-FOCSTM) to the two converters RSC and GSC of a WECS, whereas [47] propose the Modified Super Twisting (MST) algorithm for Low Voltage Ride Through (LVRT) improvement under voltage sag. The proposed algorithm is implemented using the second-order sliding mode (SOSM) to control the DFIG wind generator. Nevertheless, they have disadvantages in terms of stability and phenomena known as chattering. Despite their simplicity and robustness in principle, the practical application of SMC is limited by complex online computations and chattering problems related to control switching. Thus, these limitations considerably reduce the control performance expected from such methods in practical implementations.

On the other hand [48], design the non-linear backstepping regulator to control the active and reactive powers of the DFIG with a view to implementing the whole system using the Dspace board, while [49] confirm the robustness of the Backstepping control against parametric variations, by giving a review of the Backstepping control of a wind system based on a DFIG. Despite its design complexity, the Backstepping control algorithm, using the Lyapunov stability technique, provides a stable and robust control that achieves good performance in terms of trajectory tracking and regulation of electrical parameters, thus helping to maximize the energy production of the wind turbine system.

1.3. Contribution

Building a solid control system that oversees the proper operation of both the rotor-side and grid-side converters is important to get the most electrical output possible out of a wind power system. The nonlinear hybrid sliding mode Backstepping control law is enhanced in this study, and it is implemented on the DSPACE DS1104 board in order to validate it on a test bench in a lab with a 1.5 kW generator for a wind profile from Al Hoceima region.

The important points that this article contributes can be summed up as follows:

- Present a non-linear model based on DFIG for each component in the conversion chain for wind energy.
- Supply a method for controlling the mechanical rotational speed in order to maximize the power obtained from the wind (MPPT). The reference electromagnetic torque required to create the sliding mode Backstepping control algorithm is fundamentally provided by this.
- Explain the operational principles of the sliding mode and Backstepping control methodologies.
- Develop a robust controller design that uses a new hybrid combination of SM-Backstepping control algorithms applied to the complete wind power conversion chain based on the doubly fed induction generator, to achieve the high performance required in a wind energy system, i.e:
    - oEnsure proper monitoring of electrical reference values such as active and reactive power and DC bus voltage.
    - oBe highly robust to parametric variations, by applying the new hybrid control to the entire wind power system.
    - oTo reduce the effect of the “chattering” phenomenon as much as possible.
    - oReduce the rate of THD and improve the quality of the electrical energy fed into the grid.

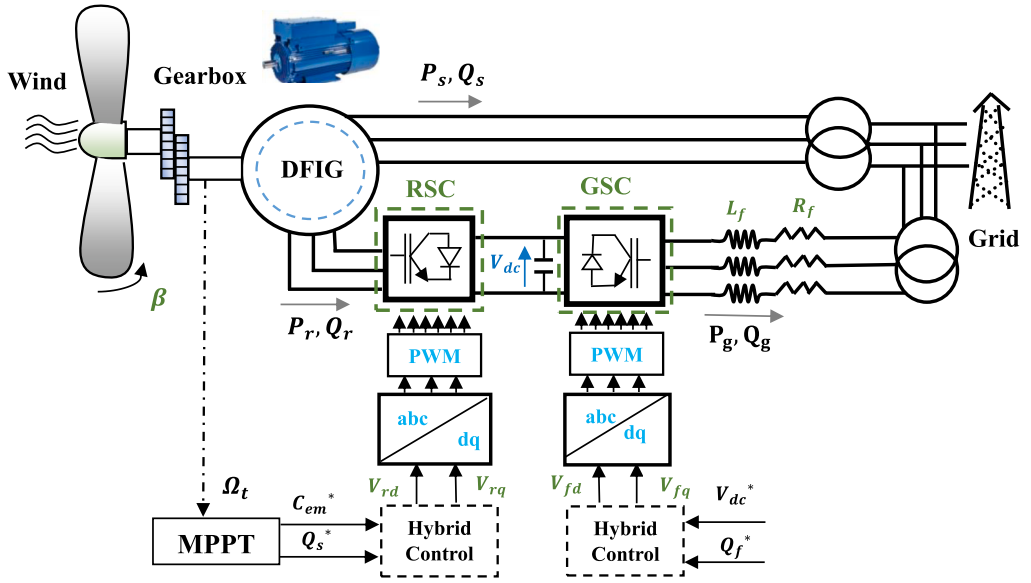

Fig. 1. The components of a wind power system's conversion chain.

- Experimentally validate the hybrid control with Matlab/Simulink software using the real wind profile of Al Hoceima region, and then confirm the effectiveness of the proposed control using a test bench consisting essentially of the DSPACE DS1104 board.

1.4. Organisation of the manuscript

This article is organised as follows: after an introduction, mathematical modelling of each element of the WECS is provided. The principle of sliding mode control is described in detail. Next, the hybrid SM-Backstepping control is well explained and applied to the rotor-side and grid-side converter. Then, the simulation results of the proposed control using the real wind profile of the AL Houceima region are presented. Finally, the whole system is implemented in real time on a test bench using the DSPACE DS1104 board and the ControlDesk in order to visualize the results obtained and verify the correct tracking of the electrical variables and the high robustness of the proposed control algorithm.

2. Mathematical modeling of a wind system

As shown in Fig. 1, the wind power system typically consists of a wind turbine, equipped with blades, which captures the kinetic energy of the wind and converts it into mechanical energy. This latter is then transmitted to the DFIG, which transforms the mechanical energy into electrical energy. The system also incorporates energy converters RSC and GSC to convert the generated direct current into alternating current, facilitating its injection into the electrical grid [50].

2.1. Wind turbine model

The turbine is modeled by the following equation (1) [51]:

$$P_{aero} = \frac{1}{2}.C_p(\lambda,\beta).\rho.\pi.R^2.V^3 \tag{1}$$

ρ: Air density (1.225 kg/m3)

$$C_p(\lambda,\beta) = 0.5176\left(\frac{116}{\gamma} - 0.4*\beta - 5\right)e^{\frac{-21}{\gamma}} + 0.0068*\lambda \tag{2}$$

With:

$$\frac{1}{\gamma} = \frac{1}{\lambda + 0.008\beta} - \frac{0.035}{\beta^3 + 1} \tag{3}$$

$$\lambda = \frac{R.\Omega_t}{V} \tag{4}$$

Fig. 2 shows the variation of the power coefficient C_p with respect to the specified speed λ and pitch angle β by modeling equations

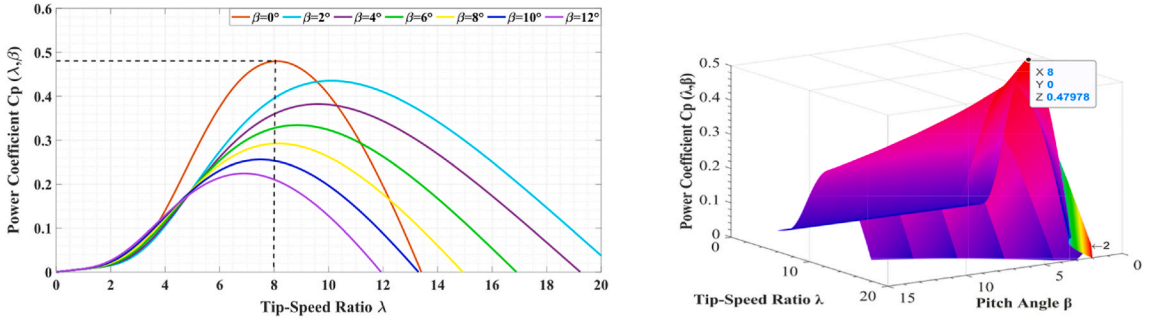

Fig. 2. The power coefficient $C_p(\lambda, \beta)$.

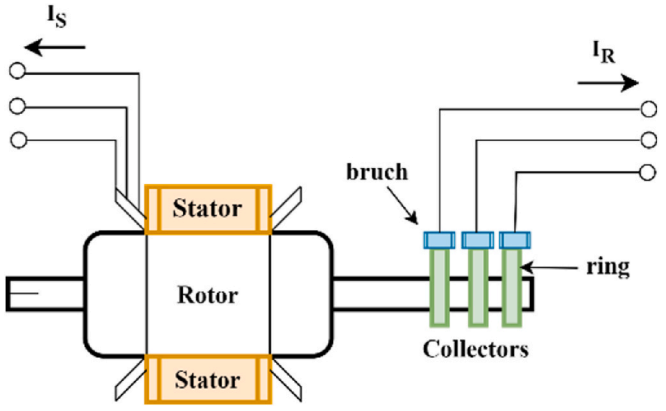

Fig. 3. The structure of DFIG.

(2)–(4) in MATLAB/Simulink. The maximum turbine efficiency for our turbine is achieved if:

$$\beta = 0\ ;\ \lambda_{opt} = 8\ ;\ C_{p-Max} = 0.479$$

Maintaining the optimal values (λ_{opt}) in the control system for variations in wind conditions is sufficient for achieving MPPT.

The reference electromagnetic torque is then obtained from the estimated torque of the wind turbine torque of the wind turbine (eq (5)):

$$C_{em-ref} = C_g = \frac{C_{t-est}}{G} \tag{5}$$

The electromagnetic reference torque must then be set to the following value (eq (6)):

$$C_{em-ref} = \frac{1}{2}.C_{p-Max}.\rho.\pi.R^5.V_{est}^3.\frac{\Omega_{mec}^2}{G^3.\lambda_{opt}^3} \tag{6}$$

The gearbox is modeled as follows [52] (eq (7)):

$$\begin{cases} \Omega_t = \dfrac{\Omega_{mec}}{G} \\ C_g = \dfrac{C_{aero}}{G} \end{cases} \tag{7}$$

The drive shaft transmits the wind turbine's rotation to the electrical part of the conversion chain. It is modeled by the following mechanical equations (eqs (8) and (9)) [53]:

$$J_{tot} = \frac{J_t}{G^2} + J_g \tag{8}$$

$$C_{mec} = J_{tot}.\frac{d\Omega_{mec}}{dt} = C_g - C_{em} - f.\Omega_{mec} \tag{9}$$

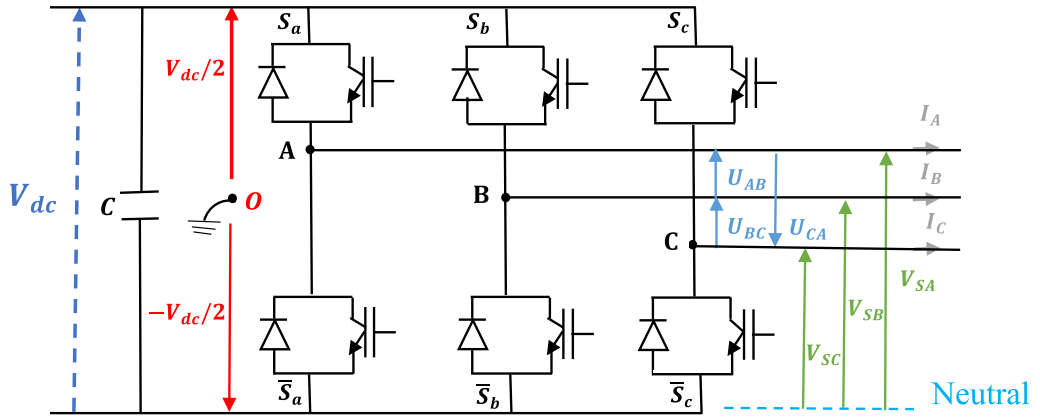

Fig. 4. Converter diagram.

2.2. DFIG model

The DFG consists of a stator, similar to that of a conventional asynchronous machine, and a rotor rotating inside the machine cavity and separated from the stator by an air gap. The three-phase winding of the rotor is accessed by three rings fitted with brushes, as shown in Fig. 3, which allow the rotor voltages to be applied by an external control system [54].

The electrical model of the DFIG in the referential (d,q) is given by:

- **Stator and rotor voltage (eqs 10 and 11)**

$$\begin{cases} V_{sd} = R_s.I_{sd} + \dfrac{d\varphi_{sd}}{dt} - \omega_s.\varphi_{sq} \\ V_{sq} = R_s.I_{sq} + \dfrac{d\varphi_{sq}}{dt} + \omega_s.\varphi_{sd} \\ V_{rd} = R_r.I_{rd} + \dfrac{d\varphi_{rd}}{dt} - \omega_r.\varphi_{rq} \\ V_{rq} = R_r.I_{rq} + \dfrac{d\varphi_{rq}}{dt} + \omega_r.\varphi_{rd} \end{cases} \tag{10}$$

$$\text{With : } \omega_r = \omega_s - p.\Omega_{mec} \tag{11}$$

-Stator and rotor flux (eqs 12 and 13)

$$\begin{cases} \varphi_{sd} = L_s.I_{sd} + M.I_{rd} \\ \varphi_{sq} = L_s.I_{sq} + M.I_{rq} \\ \varphi_{rd} = L_r.I_{rd} + M.I_{sd} \\ \varphi_{rq} = L_r.I_{rq} + M.I_{sq} \end{cases} \tag{12}$$

$$L_s = l_s - M_s, \quad L_r = l_r - M_r \tag{13}$$

-Electromagnetic torque (eq (14))

$$C_{em} = p\left(\varphi_{sd}.I_{sq} - \varphi_{sq}.I_{sd}\right) \tag{14}$$

-Active and Reactive power at stator and rotor (eq (15))

$$\begin{cases} P_s = V_{sd}.I_{sd} + V_{sq}.I_{sq}' \\ Q_s = V_{sq}.I_{sd} - V_{sd}.I_{sq}' \\ P_r = V_{rd}.I_{rd} + V_{rq}.I_{rq}' \\ Q_r = V_{rq}.I_{rd} - V_{rd}.I_{rq}' \end{cases} \tag{15}$$

2.3. Power converter model

The DFIG is a key component in the conversion chain of a wind power system. It has two windings: a rotor winding connected to the grid via two electronic converters, and a stator winding directly connected to the grid. The two converters can function as an inverter or a rectifier depending on the flow of electrical energy, and their controls allow for the management and optimization of the power generated [55,56].

The structural schema of a three-phase two-level converter is shown in Fig. 4:

All the voltages in Fig. 4 are given by the following equations (16)–(18) [57]:

$$\begin{cases} v_A = \frac{1}{3}(U_{AB} - U_{AC}) = \frac{1}{3}(2 * v_A - v_B - v_C) \\ v_B = \frac{1}{3}(U_{BC} - U_{AB}) = \frac{1}{3}(2 * v_B - v_A - v_C) \\ v_C = \frac{1}{3}(U_{CA} - U_{BC}) = \frac{1}{3}(2 * v_C - v_A - v_B) \end{cases} \tag{16}$$

$$\begin{bmatrix} v_A \\ v_B \\ v_C \end{bmatrix} = \frac{1}{3}.\begin{bmatrix} 2 & -1 & -1 \\ -1 & 2 & -1 \\ -1 & -1 & 2 \end{bmatrix}.\begin{bmatrix} v_{A0} \\ v_{B0} \\ v_{C0} \end{bmatrix} * \tag{17}$$

$$\begin{bmatrix} v_{A0} \\ v_{B0} \\ v_{C0} \end{bmatrix} = V_{dc}.\begin{bmatrix} S_a \\ S_b \\ S_c \end{bmatrix} - \frac{V_{dc}}{2} \tag{18}$$

The state of the switches, assumed to be perfect, can be defined by three Boolean control variables Si ($i = a,b,c$):

- $S_i = 1$, the case where the upper switch is closed and the lower switch is open.
- $S_i = 0$, the case where the top switch is open and the bottom switch is closed.

Under these conditions, simple voltages can be written in the following matrix form (eq (19)):

$$\begin{bmatrix} v_A \\ v_B \\ v_C \end{bmatrix} = \frac{V_{dc}}{3}.\begin{bmatrix} 2 & -1 & -1 \\ -1 & 2 & -1 \\ -1 & -1 & 2 \end{bmatrix}.\begin{bmatrix} S_a \\ S_b \\ S_c \end{bmatrix} \tag{19}$$

The use of this type of converter makes it possible to obtain Pulse Width Modulation output signal shapes whose modularity makes it possible to limit interference by modifying the frequency spectrum of the signal (rejection of the first non-zero harmonics towards high frequencies).

2.4. DC bus model

The time evolution of the DC bus voltage is obtained from the following integration (eq (20)) [58]:

$$\begin{cases} W_{dc} = \int P_c \,.\, dt = \frac{1}{2}.C.{V_{dc}}^2 \\ \frac{d{V_{dc}}^2}{dt} = \frac{2}{C}(P_f - P_r) \end{cases} \tag{20}$$

2.5. RL filter model

The voltage equations modeling the filter are written in PARK's reference frame (d,q) as follows (eq (21)) [59]:

$$\begin{cases} v_{fd} = -R_f.I_{fd} - L_f.\frac{dI_{fd}}{dt} + \omega_s.L_f.I_{fq} \\ v_{fq} = -R_f.I_{fq} - L_f.\frac{dI_{fq}}{dt} - \omega_s.L_f.I_{fd} + v_s \end{cases} \tag{21}$$

3. Theory of sliding mode control

The central idea behind SMC is to create a sliding surface, a hyperplane in state space, along which the system's state trajectory should ideally "slide". The sliding surface is defined by an equation or set of equations that relate the system's states. SMC passes through three stages [60]:

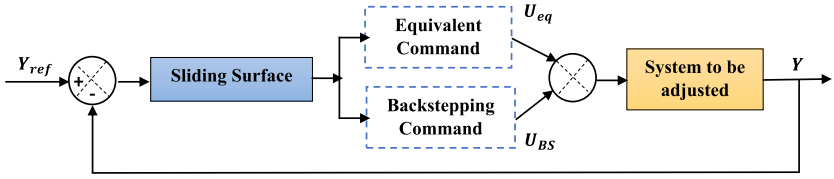

Fig. 5. The sliding-backstepping mode Controller's composition.

- The choice of the sliding surface (eq (22))

$$\boldsymbol{S(x) = \left(\frac{d}{dt} + \delta\right)^{r-1} . e(x)} \text{ “} \tag{22}$$

- The establishment of conditions of existence

In order to ensure both the stability of the non-linear system and the attraction of the variable to be regulated towards its reference value, LYAPUNOV proposes a $V(x)$ function (eqs (23) and (24)) [61]:

$$V(x) = \frac{1}{2} .S(x)^2 \tag{23}$$

$$\dot{V}(x) = S(x) * \dot{S}(x) < 0 \tag{24}$$

- The control law's determination

Two terms make up the sliding mode control (eq (25)) [62]:

$$u = u_{eq} + u_n \tag{25}$$

u_{eq}: this vector describes an ideal slip movement independent of the uncertainties and disturbances generated by the system. The following invariance conditions for the slip surface give its expression (eq (26)):

$$\begin{cases} \dot{S}(x) = 0 \\ S(x) = 0 \end{cases} \tag{26}$$

For discontinuous control, the simplest of those found in the literature is as follows (eq (27)) [63]:

$$u_n = K.sign(S(x)) \tag{27}$$

K: the control gain

The sign function returns -1, 0 or $+1$ when the numeric expression value is negative, zero or positive.

Although sliding mode control has several advantages, it also has a disadvantage known as “chattering”, which can lead to unwanted vibrations due to rapid and frequent variations in control around the sliding surface [64].

4. Hybrid sliding-backstepping mode control

In this paper, a new technique is developed to overcome the chattering drawback of SMC in the pursuit of higher performance. Hybrid sliding mode backstepping is the term used to describe this method as shown in Fig. 5.

SMC and BSC are the two control approaches on which the hybrid sliding-backstepping control theory is built. By guiding the system along a predefined sliding surface, SMC tries to make the system insensitive to shocks and uncertainty. The difference between the system's actual output and the desired reference output is used to define this sliding surface. The goal is to use a suitable control law to force the system to stay on this sliding surface. As a result, the system is resistant to errors and changes in the system [65].

BSC, on the other hand, is a control technique that involves designing a series of control laws by working “backwards” through the system dynamics. Each step in the backstepping process adds a control term that cancels out previous errors and leads the system towards a desired reference trajectory. The aim is to design sequential control laws that stabilize the system and lead it towards precise trajectory-following performance [66].

In hybrid Sliding-Backstepping control, sliding mode control is used to maintain the system in a finite-slip subspace. When the system reaches this space, backstepping control is activated to guide the system to the desired reference trajectory using specific control laws.

By combining these two techniques, hybrid Sliding-Backstepping control offers both robustness to disturbances and uncertainties and high trajectory-following accuracy.

5. Rotor side converter control

- Determining the equivalent control V_{rdeq} and V_{rqeq}

Applying SMC to the DFIG (eqs (28) and (29)) [67]:

$$\begin{cases} e_1 = P_{sref} - P_s \\ e_2 = Q_{sref} - Q_s \end{cases} \tag{28}$$

$$\begin{cases} \dot{e}_1 = \dot{P}_{sref} - \dot{P}_s \\ \dot{e}_2 = \dot{Q}_{sref} - \dot{Q}_s \end{cases} \tag{29}$$

With (eq (30) and (31)):

$$\begin{cases} \dot{P}_s = -\dfrac{v_s.M}{L_s}\dot{I}_{rq} \\ \dot{Q}_s = \dfrac{v_s^2}{\omega_s.L_s} - \dfrac{v_s.M}{L_s}\dot{I}_{rd} \\ \dot{I}_{rd} = \dfrac{V_{rd}}{L_r.\sigma} - \dfrac{R_r}{L_r.\sigma}.I_{rd} + \omega_r.I_{rq} \\ \dot{I}_{rq} = \dfrac{V_{rq}}{L_r.\sigma} - \dfrac{R_r}{L_r.\sigma}.I_{rq} - \omega_r.I_{rd} - \omega_r.\dfrac{M.V_s}{L_r.L_s.\sigma.\omega_s} \end{cases} \tag{30}$$

$$\begin{cases} \dot{e}_1 = \dot{P}_{sref} + \dfrac{V_s.M}{L_s}\left(\dfrac{V_{rq}}{L_r.\sigma} - \dfrac{R_r}{L_r.\sigma}.I_{rq} - \omega_r.I_{rd} - \omega_r.\dfrac{M.V_s}{L_r.L_s.\sigma.\omega_s}\right) \\ \dot{e}_2 = \dot{Q}_{sref} + \dfrac{V_s.M}{L_s}\left(\dfrac{V_{rd}}{L_r.\sigma} - \dfrac{R_r}{L_r.\sigma}.I_{rd} + \omega_r.I_{rq}\right) \end{cases} \tag{31}$$

As already mentioned, the sliding mode controller consists of two terms (eq (32)):

$$U = U_{eq} + U_n \tag{32}$$

As a result, the following gives the expression for the derivative of the sliding surface (eq (33)):

$$\begin{cases} \dot{e}_1 = \dot{P}_{sref} + \dfrac{V_s.M}{L_s}\left(\dfrac{\boldsymbol{V_{rqeq}} + \boldsymbol{V_{rqn}}}{L_r.\sigma} - \dfrac{R_r}{L_r.\sigma}.I_{rq} - \omega_r.I_{rd} - \omega_r.\dfrac{M.V_s}{L_r.L_s.\sigma.\omega_s}\right) \\ \dot{e}_2 = \dot{Q}_{sref} + \dfrac{V_s.M}{L_s}\left(\dfrac{\boldsymbol{V_{rdeq}} + \boldsymbol{V_{rdn}}}{L_r.\sigma} - \dfrac{R_r}{L_r.\sigma}.I_{rd} + \omega_r.I_{rq}\right) \end{cases} \tag{33}$$

During sliding mode and permanent mode, we have (eq (34)):

$$\begin{cases} e_{1,2} = 0 \\ \dot{e}_{1,2} = 0 \\ V_{rdn} = V_{rqn} = 0 \end{cases} \tag{34}$$

The expression for the derivative of the sliding surface becomes (eq (35)):

$$\begin{cases} \boldsymbol{V_{rdeq}} = -\dfrac{\boldsymbol{L_r.L_s.\sigma}}{\boldsymbol{M.V_s}}.\dot{\boldsymbol{Q}}_{\boldsymbol{sref}} + \boldsymbol{R_r.I_{rd}} - \boldsymbol{\omega_r.L_r.\sigma.I_{rq}} \\ \boldsymbol{V_{rqeq}} = -\dfrac{\boldsymbol{L_r.L_s.\sigma}}{\boldsymbol{M.V_s}}.\dot{\boldsymbol{P}}_{\boldsymbol{sref}} + \boldsymbol{R_r.I_{rq}} + \boldsymbol{\omega_r.L_r.\sigma.I_{rd}} + \boldsymbol{\omega_r.V_s}.\dfrac{\boldsymbol{M}}{\boldsymbol{L_s.\omega_s}} \end{cases} \tag{35}$$

- Determining the discontinuous control V_{rdn} and V_{rqn}

The RSC is subjected to the backstepping control:
Calculating reference rotor currents is the first step.
The following equation gives the Lyapunov function connected to the stator's active and reactive power errors (eq (36)) [68]:

$$V_1 = \frac{1}{2}.e_1^2 + \frac{1}{2}.e_2^2 \tag{36}$$

Its derivative is stated as follows:

$$\dot{V}_1 = e_1.\dot{e}_1 + e_2.\dot{e}_2 = e_1\left[\dot{P}_{sref} + \frac{V_s.M}{L_r.\sigma.L_s}\left(V_{rq} - R_r.I_{rq} - L_r.\sigma.\omega_r.I_{rd} - g.\frac{M.V_s}{L_s}\right)\right] + e_2\left[\dot{Q}_{sref} + \frac{V_s.M}{L_r.\sigma.L_s}\left(V_{rd} - R_r.I_{rd} + L_r.\sigma.\omega_r.I_{rq}\right)\right] \tag{37}$$

According to Lyapunov, $\dot{V}_1$ must be negative in order to guarantee the stability of the subsystem. For this, we select it in the following format:

$$\dot{V}_1 = -k_1.e_1^2 - k_2.e_2^2 \leq 0 \tag{38}$$

When equations (37) and (38) are equivalent, the following result is obtained (eq (39)):

$$e_1\left[\dot{P}_{sref} + \frac{V_s.M}{L_r.\sigma.L_s}\left(V_{rq} - R_r.I_{rq} - L_r.\sigma.\omega_r.I_{rd} - g.\frac{M.V_s}{L_s}\right)\right] + e_2\left[\dot{Q}_{sref} + \frac{V_s.M}{L_r.\sigma.L_s}\left(V_{rd} - R_r.I_{rd} + L_r.\sigma.\omega_r.I_{rq}\right)\right] = -k_1.e_1^2 - k_2.e_2^2 \tag{39}$$

Which give: (eq (40))

$$\begin{cases} e_1\left[\dot{P}_{sref} + \frac{V_s.M}{L_r.\sigma.L_s}\left(V_{rq} - R_r.I_{rq} - L_r.\sigma.\omega_r.I_{rd} - g.\frac{M.V_s}{L_s}\right)\right] = -k_1.e_1^2 \\ e_2\left[\dot{Q}_{sref} + \frac{V_s.M}{L_r.\sigma.L_s}\left(V_{rd} - R_r.I_{rd} + L_r.\sigma.\omega_r.I_{rq}\right)\right] = -k_2.e_2^2 \end{cases} \tag{40}$$

The following defines the expression of the virtual control I_{rd} and I_{rq} (eq (41)):

$$\begin{cases} I_{rqref} = \left[\frac{L_r.\sigma.L_s}{R_r.V_s.M}\left(\dot{P}_{sref} + k_1.e_1 + \frac{V_s.M}{L_r.\sigma.L_s}\left(V_{rq} - L_r.\sigma.\omega_r.I_{rd} - g.\frac{M.V_s}{L_s}\right)\right)\right]^* \\ I_{rdref} = \frac{L_r.\sigma.L_s}{R_r.V_s.M}\left[\dot{Q}_{sref} + k_2.e_2 + \frac{V_s.M}{L_r.\sigma.L_s}\left(V_{rd} + L_r.\sigma.\omega_r.I_{rq}\right)\right] \end{cases}^* \tag{41}$$

Calculating the rotor voltages in step two.
We shall derive the real control laws V_{rqn} and V_{rdn} that allow the system's design goals to be fulfilled.
The rotor current errors are determined according to the criteria below (eq (42)) [69]:

$$\begin{cases} e_3 = I_{rqref} - I_{rq} \\ e_4 = I_{rdref} - I_{rd} \end{cases} \tag{42}$$

Their derivatives are given by (eq (43)):

$$\begin{cases} \dot{e}_3 = \dot{I}_{rqref} - \dot{I}_{rq} \\ \dot{e}_4 = \dot{I}_{rdref} - \dot{I}_{rd} \end{cases} \tag{43}$$

So (eq (44)):

$$\begin{cases} \dot{e}_3 = \dot{I}_{rqref} - \frac{1}{L_r.\sigma}\left(V_{rqn} - R_r.I_{rq} - L_r.\sigma.\omega_r.I_{rd} - g.\frac{M.V_s}{L_s}\right. \\ \dot{e}_4 = \dot{I}_{rdref} - \frac{1}{L_r.\sigma}\left(V_{rdn} - R_r.I_{rd} + L_r.\sigma.\omega_r.I_{rq}\right. \end{cases} \tag{44}$$

The expanded Lyapunov function takes on the following form (eq (45)):

$$V_2 = \frac{1}{2}.e_1^2 + \frac{1}{2}.e_2^2 + \frac{1}{2}.e_3^2 + \frac{1}{2}.e_4^2 \tag{45}$$

The derivative of it is as follows (eq (46)):

$$\dot{V}_2 = e_1.\dot{e}_1 + e_2.\dot{e}_2 + e_3.\dot{e}_3 + e_4.\dot{e}_4 \tag{46}$$

Which give (eq (47)):

$$\dot{V}_2 = \dot{V}_1 + e_3.\dot{e}_3 + e_4.\dot{e}_4 \tag{47}$$

$$\dot{V}_2 = \dot{V}_1 + e_3\left[\dot{I}_{rqref} - \frac{1}{L_r.\sigma}\left(V_{rqn} - R_r.I_{rq} - L_r.\sigma.\omega_r.I_{rd} - g.\frac{M.V_s}{L_s}\right)\right] + e_4\left[\dot{I}_{rdref} - \frac{1}{L_r.\sigma}\left(V_{rdn} - R_r.I_{rd} + L_r.\sigma.\omega_r.I_{rq}\right)\right] \tag{48}$$

For the system to be stable, $\dot{V}_2$ must be negative. In order to do this, we select $\dot{V}_2$ in the form [70]:

$$\dot{V}_2 = -k_1.e_1^2 - k_2.e_2^2 - k_3.e_3^2 - k_4.e_4^2 = \dot{V}_1 - k_3.e_3^2 - k_4.e_4^2 \leq 0 \tag{49}$$

By equating these two equations (48) and (49), we obtain (eq (50)):

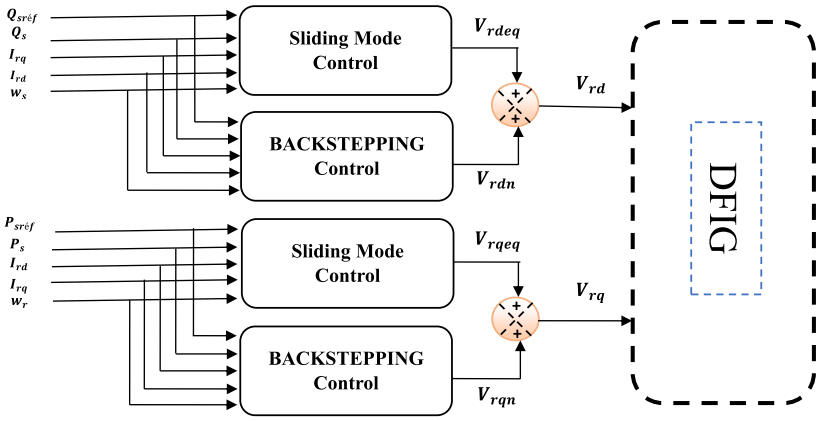

Fig. 6. Application of hybrid control on the RSC.

$$\dot{V}_1 - k_3.e_3^2 - k_4.e_4^2 = \dot{V}_1 + e_3\left[\dot{I}_{rqref} - \frac{1}{L_r.\sigma}\left(V_{rqn} - R_r.I_{rq} - L_r.\sigma.\omega_r.I_{rd} - g.\frac{M.V_s}{L_s}\right)\right] + e_4\left[\dot{I}_{rdref} - \frac{1}{L_r.\sigma}\left(V_{rdn} - R_r.I_{rd} + L_r.\sigma.\omega_r.I_{rq}\right)\right] \tag{50}$$

So (eq (51)):

$$\begin{cases} e_3\left[\dot{I}_{rqref} - \frac{1}{L_r.\sigma}\left(V_{rqn} - R_r.I_{rq} - L_r.\sigma.\omega_r.I_{rd} - g.\frac{M.V_s}{L_s}\right)\right] = -k_3.e_3^2 \\ e_4\left[\dot{I}_{rdref} - \frac{1}{L_r.\sigma}\left(V_{rdn} - R_r.I_{rd} + L_r.\sigma.\omega_r.I_{rq}\right)\right] = -k_4.e_4^2 \end{cases} \tag{51}$$

This provides the formulation of the true global control, V_{rdn} and V_{rqn} defined by (eq (52)):

$$\begin{cases} \boldsymbol{V_{rdn} = L_r.\sigma\left[k_4.e_4 + \dot{I}_{rdref} + \frac{1}{L_r.\sigma}\left(R_r.I_{rd} - L_r.\sigma.\omega_r.I_{rq}\right)\right]} \\ \boldsymbol{V_{rqn} = L_r.\sigma\left[k_3.e_3 + \dot{I}_{rqref} + \frac{1}{L_r.\sigma}\left(R_r.I_{rq} + L_r.\sigma.\omega_r.I_{rd} + g.\frac{M.V_s}{L_s}\right)\right]} \end{cases} \tag{52}$$

With: k_3, k_4 are positive constants.

- **Global Control generation using Sliding-Backstepping Mode control**

The first term "u_{eq}" produced by the sliding-mode control and the second term "u_n" produced by the backstepping control constitute the hybrid sliding-backstepping mode controller for the two rotor voltage vectors V_{rd} and V_{rq} as shown in Fig. 6 and (eqs (53) and (54)).

$$u_{MG-BS} = u_{eq-MG} + u_{n-BS} \tag{53}$$

$$\begin{cases} \boldsymbol{V_{rd} = -\frac{L_r.L_s.\sigma}{M.V_s}.\dot{Q}_{sref} + R_r.I_{rd} - L_r.\sigma.\omega_r.I_{rq} + L_r.\sigma\left[k_4.e_4 + \dot{I}_{rdref} + \frac{1}{L_r.\sigma}\left(R_r.I_{rd} - L_r.\sigma.\omega_r.I_{rq}\right)\right]} \\ \boldsymbol{V_{rq} = -\frac{L_r.L_s.\sigma}{M.V_s}.\dot{P}_{sref} + R_r.I_{rq} + L_r.\sigma.\omega_r.I_{rd} + \omega_r.\frac{M.V_s}{L_s.\omega_s} + L_r.\sigma\left[k_3.e_3 + \dot{I}_{rqref} + \frac{1}{L_r.\sigma}\left(R_r.I_{rq} + L_r.\sigma.\omega_r.I_{rd} + g.\frac{M.V_s}{L_s}\right)\right]} \end{cases} \tag{54}$$

6. Grid side converter control

-Determining the equivalent control V_{fdeq} and V_{fqeq}

Applying sliding-mode control to the DFIG for $r = 1$, the active and reactive power slip area is given by Ref. [71] (eq (55)):

$$\begin{cases} e_5 = P_{fref} - P_f \\ e_6 = Q_{fref} - Q_f \end{cases}' \tag{55}$$

The errors' derivatives are as follows (eq (56)):

$$\begin{cases} \dot{e}_5 = \dot{P}_{fref} - \dot{P}_f \\ \dot{e}_6 = \dot{Q}_{fqref} - \dot{Q}_{fq} \end{cases} \tag{56}$$

With (eqs (57) and (58)):

$$\begin{cases} P_f = v_s.I_{fq} \\ Q_f = -v_s.I_{fd} \\ \dot{I}_{fq} = -\dfrac{v_{fq}}{L_f} - \dfrac{R_f}{L_f}.I_{fq} - \omega_s.I_{fd} + \dfrac{v_s}{L_f} \\ \dot{I}_{fd} = -\dfrac{v_{fd}}{L_f} - \dfrac{R_f}{L_f}.I_{fd} + \omega_s.I_{fq} \end{cases} \tag{57}$$

$$\begin{cases} \dot{e}_5 = \dot{P}_{fref} - v_s\left(-\dfrac{v_{fq}}{L_f} - \dfrac{R_f}{L_f}.I_{fq} - \omega_s.I_{fd} + \dfrac{v_s}{L_f}\right) \\ \dot{e}_6 = \dot{Q}_{fref} + v_s.\left(-\dfrac{v_{fd}}{L_f} - \dfrac{R_f}{L_f}.I_{fd} + \omega_s.I_{fq}\right) \end{cases} \tag{58}$$

The derivative of the sliding surface becomes (eq (59)):

$$\begin{cases} \dot{e}_5 = \dot{P}_{fref} + \dfrac{v_s.R_f}{L_f}.I_{fq} + \dfrac{v_s\left(v_{fqeq} + v_{fqn}\right)}{L_f} + v_s.\omega_s.I_{fd} - \dfrac{{v_s}^2}{L_f} \\ \dot{e}_6 = \dot{Q}_{fref} - \dfrac{v_s.R_f}{L_f}.I_{fd} - \dfrac{v_s\left(v_{fdeq} + v_{fdn}\right)}{L_f} + v_s.\omega_s.I_{fq} \end{cases} \tag{59}$$

In sliding and permanent mode, we get the equivalent control expressed by (eq (60)):

$$\begin{cases} \boldsymbol{V_{fdeq}} = \dfrac{\boldsymbol{L_f}}{\boldsymbol{V_s}}.\dot{\boldsymbol{Q}}_{\boldsymbol{sref}} - \boldsymbol{R_f}.\boldsymbol{I_{fd}} + \boldsymbol{L_f}.\boldsymbol{\omega_s}.\boldsymbol{I_{fq}} \\ \boldsymbol{V_{fqeq}} = \dfrac{\boldsymbol{L_f}}{\boldsymbol{V_s}}.\dot{\boldsymbol{P}}_{\boldsymbol{sref}} - \boldsymbol{R_f}.\boldsymbol{I_{fq}} - \boldsymbol{L_f}.\boldsymbol{\omega_s}.\boldsymbol{I_{fd}} + \boldsymbol{V_s} \end{cases} \tag{60}$$

-Determining the discontinuous control V_{fdn} and V_{fqn}

The GSC is subjected to the Backstepping control:
Calculate the $\boldsymbol{I_{fd}}$ and $\boldsymbol{I_{fq}}$ filter currents in step one
The following equation describes the Lyapunov function linked to the filter's active and reactive power errors (eq (61)):

$$V_3 = \frac{1}{2}.e_5^2 + \frac{1}{2}.e_6^2 \tag{61}$$

The derivative of it is as follows:

$$\dot{V}_3 = e_5.\dot{e}_5 + e_6.\dot{e}_6 = e_5\left(\dot{P}_{fref} - v_s\left(-\frac{v_{fqn}}{L_f} - \frac{R_f}{L_f}.I_{fq} - \omega_s.I_{fd} + \frac{v_s}{L_f}\right)\right) + e_6\left(\dot{Q}_{fref} + v_s\left(-\frac{v_{fdn}}{L_f} - \frac{R_f}{L_f}.I_{fd} + \omega_s.I_{fq}\right)\right) \tag{62}$$

For the system to be stable, $\dot{V}_3$ must be negative. In order to do this, we select $\dot{V}_3$ in the form [72]:

$$\dot{V}_3 = -k_5.e_5^2 - k_6.e_6^2 \leq 0* \tag{63}$$

With: k_5, k_6 are positive constants
By equating these two equations (62) and (63), we get (eq (64)):

$$e_5\left(\dot{P}_{fref} - v_s\left(-\frac{v_{fqn}}{L_f} - \frac{R_f}{L_f}I_{fq} - \omega_s.I_{fd} + \frac{v_s}{L_f}\right)\right) + e_6\left(\dot{Q}_{fref} + v_s.\left(-\frac{v_{fdn}}{L_f} - \frac{R_f}{L_f}.I_{fd} + \omega_s.I_{fq}\right)\right) = -k_5.e_5^2 - k_6.e_6^2 \tag{64}$$

Which give (eq (65)):

$$\begin{cases} e_5\left(\dot{P}_{fref} - v_s\left(-\dfrac{v_{fqn}}{L_f} - \dfrac{R_f}{L_f}.I_{fq} - \omega_s.I_{fd} + \dfrac{v_s}{L_f}\right)\right) = -k_5.e_5^2 \\ e_6\left(\dot{Q}_{fref} + v_s.\left(-\dfrac{v_{fdn}}{L_f} - \dfrac{R_f}{L_f}.I_{fd} + \omega_s.I_{fq}\right)\right) = -k_6.e_6^2 \end{cases} \tag{65}$$

The following defines the expression of the virtual control I_{fd} and I_{fq} (eq (66)):

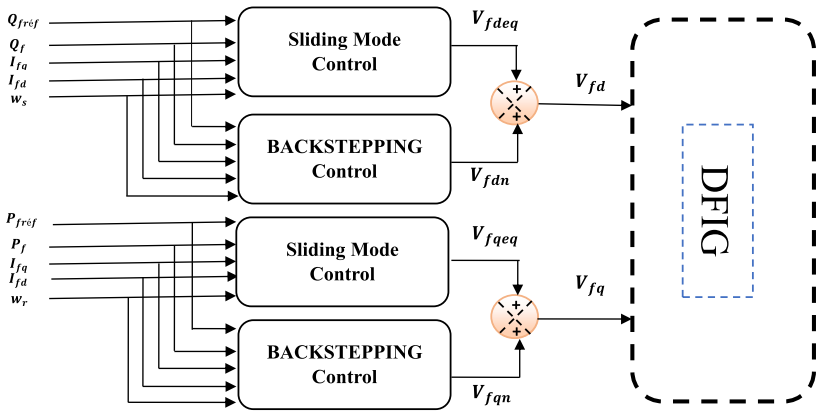

Fig. 7. Application of hybrid control on the GSC.

$$\begin{cases} I_{fqref} = -\dfrac{L_f}{R_f.v_s}\left(\dot{P}_{fref} + v_s\left(\dfrac{v_{fqn}}{L_f} + \omega_s.I_{fd} - \dfrac{v_s}{L_f}\right) + k_5.e_5\right) \\ I_{fdref} = \dfrac{L_f}{R_f.v_s}.\left(\dot{Q}_{fref} + v_s.\left(-\dfrac{v_{fdn}}{L_f} + \omega_s.I_{fq}\right) + k_6.e_6\right) \end{cases} \tag{66}$$

The upcoming system's preferred reference will be this control.
Calculating the filter voltages in step two $\boldsymbol{V_{fdn}}$ and $\boldsymbol{V_{fqn}}$
To accomplish the design goals for the entire system, we shall deduce the genuine control laws V_{fdn} and V_{fqn} in this stage (eq (67)).

$$\begin{cases} e_7 = I_{fdref} - I_{fd} \\ e_8 = I_{fqref} - I_{fq} \end{cases} \tag{67}$$

The derivatives of the errors are provided by (eqs (68) and (69)):

$$\begin{cases} \dot{e}_7 = \dot{I}_{fdref} - \dot{I}_{fd} \\ \dot{e}_8 = \dot{I}_{fqref} - \dot{I}_{fq} \end{cases} \tag{68}$$

$$\begin{cases} \dot{e}_7 = \dot{I}_{fdref} + \dfrac{v_{fdn}}{L_f} + \dfrac{R_f}{L_f}.I_{fd} - \omega_s.I_{fq} \\ \dot{e}_8 = \dot{I}_{fqref} + \dfrac{v_{fqn}}{L_f} + \dfrac{R_f}{L_f}.I_{fq} + \omega_s.I_{fd} - \dfrac{v_s}{L_f} \end{cases} \tag{69}$$

The "LYAPUNOV" function is given as follows (eq (70)):

$$V_4 = \frac{1}{2}.e_7^2 + \frac{1}{2}.e_8^2 \tag{70}$$

The derivative of it is as follows:

$$\dot{V}_4 = e_7.\dot{e}_7 + e_8.\dot{e}_8 = e_7\left(\dot{I}_{fdref} + \frac{v_{fdn}}{L_f} + \frac{R_f}{L_f}.I_{fd} - \omega_s.I_{fq}\right) + e_8\left(\dot{I}_{fqref} + \frac{v_{fqn}}{L_f} + \frac{R_f}{L_f}.I_{fq} + \omega_s.I_{fd} - \frac{v_s}{L_f}\right) \tag{71}$$

According to LYAPUNOV, in order to guarantee the stability of the system, a negative function, $\dot{V}_4$, must be used. We select $\dot{V}_4$ in the following format for this [73]:

$$\dot{V}_4 = -k_7.e_7^2 - k_8.e_8^2 \leq 0 \tag{72}$$

With: k_7, k_8 are positive constants.

By equating these two equations (71) and (72), we obtain:

$$e_7\left(\dot{I}_{fdref} + \frac{v_{fdn}}{L_f} + \frac{R_f}{L_f}.I_{fd} - \omega_s.I_{fq}\right) + e_8\left(\dot{I}_{fqref} + \frac{v_{fqn}}{L_f} + \frac{R_f}{L_f}.I_{fq} + \omega_s.I_{fd} - \frac{v_s}{L_f}\right) = -k_7.e_7^2 - k_8.e_8^2 \tag{73}$$

Which give (eq (74)):

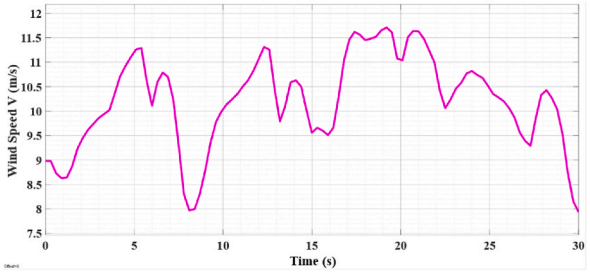

Fig. 8. Al Hoceima Morocco's variable wind speed profile.

Table 1
Abbreviations.

MPPT	**Maximum Power Point Tracking**	BSC	Backstepping Control
DFIG	Doubly Fed Induction Generator	**DPC**	Direct Power Control
RSC	Rotor Side Converter	**DTC**	Direct Torque Control
GSC	Grid Side Converter	**PI**	Proportional Integral
FOC	Field Oriented Control	**WECS**	Wind Energy Conversion System
IFOC	Indirect Field Oriented Control	**THD**	Total Harmonic Distortion
SMC	Sliding Mode Control	**PWM**	Pulse Width Modulation

$$\begin{cases} e_7\left(\dot{I}_{fdref}+\dfrac{v_{fdn}}{L_f}+\dfrac{R_f}{L_f}.I_{fd}-\omega_s.I_{fq}\right)=-k_7.e_7^2 \\ e_8\left(\dot{I}_{fqref}+\dfrac{v_{fqn}}{L_f}+\dfrac{R_f}{L_f}.I_{fq}+\omega_s.I_{fd}-\dfrac{v_s}{L_f}\right)=-k_8.e_8^2 \end{cases} \tag{74}$$

The expression of the global real control V_{fdn} and V_{fqn} defined by (eq (75)):

$$\begin{cases} \boldsymbol{v_{fdn}=-L_f\left(k_7.e_7+\dot{I}_{fdref}+\dfrac{R_f}{L_f}.I_{fd}+\omega_s.I_{fq}\right)} \\ \boldsymbol{v_{fqn}=-L_f\left(k_8.e_8+\dot{I}_{fqref}+\dfrac{R_f}{L_f}.I_{fq}+\omega_s.I_{fd}-\dfrac{v_s}{L_f}\right)} \end{cases} \tag{75}$$

- **Global Control Generation through Sliding-Backstepping Mode Control**

According to Fig. 7, the hybrid sliding-backstepping mode controller for the two filter voltage vectors V_{fd} and V_{fq} is made up of the first term " u_{eq}" produced by the sliding-mode control and the second term " u_n" produced by the Backstepping control (eqs (76) and (77)).

$$u_{MG-BS}=u_{eq-MG}+u_{n-BS}' \tag{76}$$

So:

$$\begin{cases} \boldsymbol{v_{fd}=\dfrac{L_f}{V_s}.\dot{Q}_{sref}-R_f.I_{fd}+L_f.I_{fq}.\omega_s-L_f\left(k_5.e_5+\dot{I}_{fdref}+\dfrac{R_f}{L_f}.I_{fd}+\omega_s.I_{fq}\right)} \\ \boldsymbol{v_{fq}=\dfrac{L_f}{V_s}.\dot{P}_{sref}-R_f.I_{fq}-L_f.I_{fd}.\omega_s+v_s-L_f\left(k_6.e_6+\dot{I}_{fqref}+\dfrac{R_f}{L_f}.I_{fq}+\omega_s.I_{fd}-\dfrac{v_s}{L_f}\right)} \end{cases} \tag{77}$$

7. Results of simulation

In order to test and validate the control developed above, two tests were carried out:

The first test concerns the monitoring and regulation of the wind power system, taking the aerodynamic power according to the MPPT strategy as the reference for the active power of the DFIG stator and zero as the reference for the reactive power of the stator, in order to guarantee a unitary power factor on the stator side and therefore optimize the quality of the energy returned to the grid.

The second test aims at evaluating the robustness of the control with respect to parametric variations. In this section, a real wind profile from AL Hoceima region on the north coast of Morocco is shown in Fig. 8, applied to a wind system based on a 1.5 kW DFIG (Table 1). Simulation results for the two tests are given in Figs. 9 and 10 respectively.

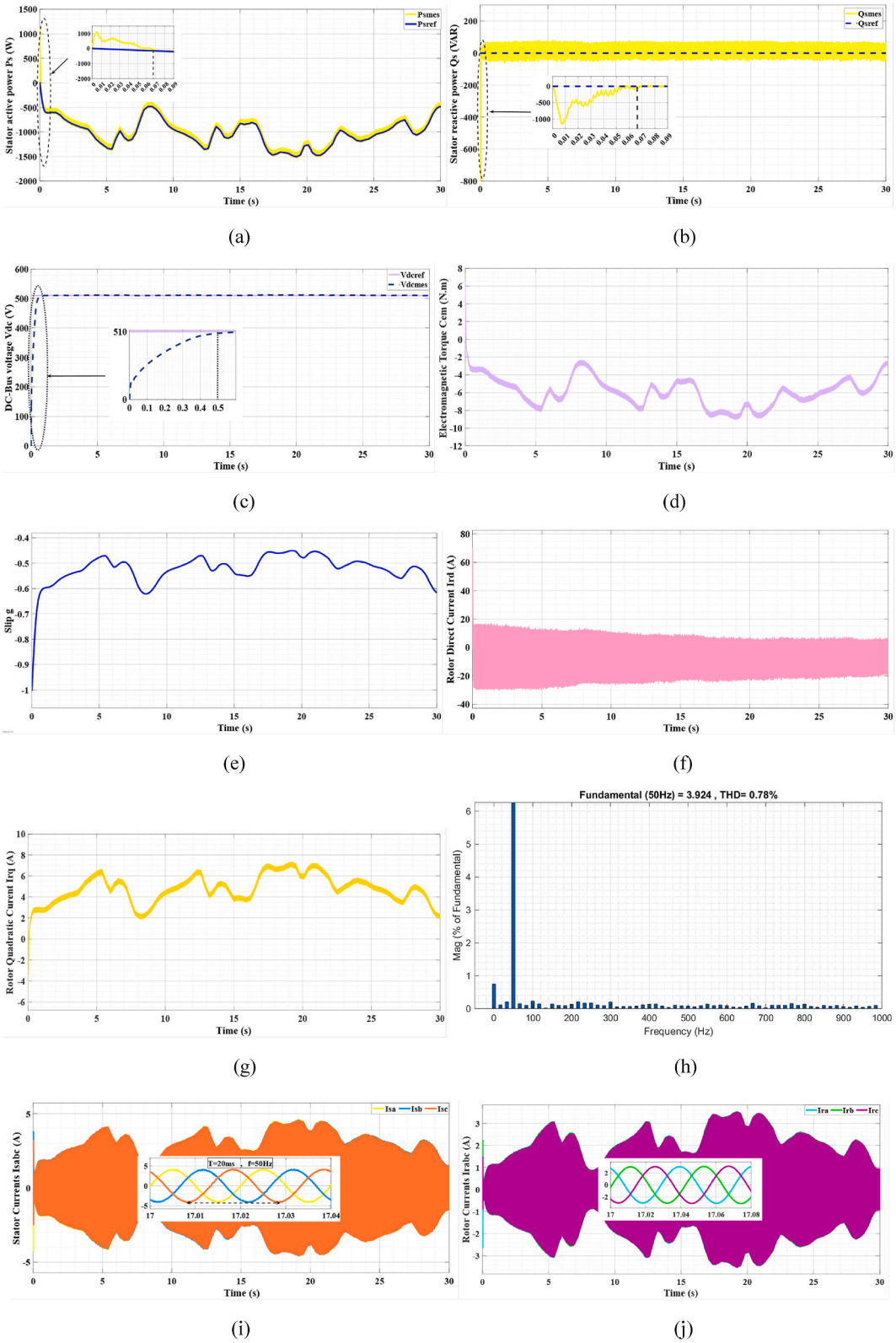

Fig. 9. Simulation results for hybrid control of a wind power system based on DFIG: (a) Active Power P_s, (b) Reactive power Q_s, (c) DC Bus voltage V_{dc}, (d) Electromagnetic Torque C_{em}, (e) Slip g, (f) Direct current I_{rd}, (g) Quadratic current I_{rq}, (h) Stator currents THD, (i) Stator currents I_{sabc}, (j) rotor currents i_{rabc}.

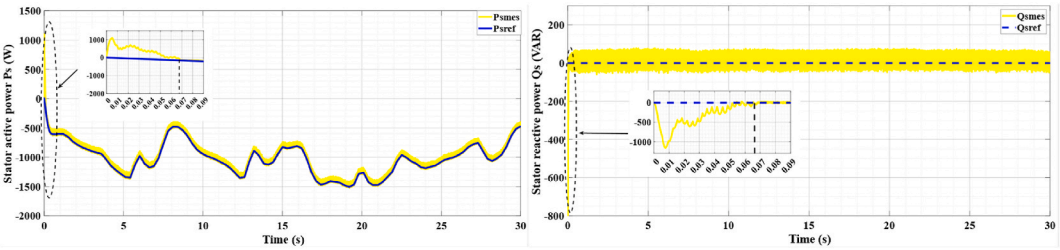

Fig. 10. Robustness test with variation of resistances Rr and Rs for variable wind speed.

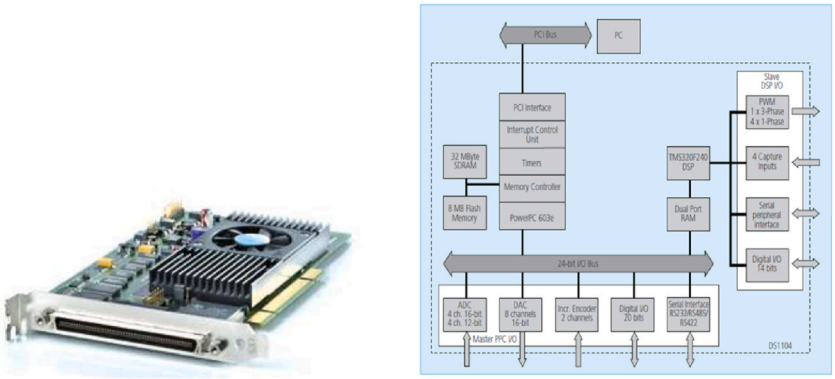

Fig. 11. Illustration of the DS1104 Board and DS1104 architecture.

- **Pursuit Tests for Variable speed response**

The active power has the same inverse shape as the wind profile, and the fact that the machine is operating in generator mode explains the negative sign of the active power. It follows its reference from time $t = 0.069s$ as shown in Fig. 9 (a) with almost no deviation. While the reactive power follows its zero reference with a response time of $0.069s$ as shown in Fig. 9 (b) with a small error.

With regard to the VDC response, Fig. 9 (c) shows that the DC bus voltage requires $0.5s$ to achieve the constant reference value of $510V$. While Fig. 9 (d) shows the electromagnetic torque varying inversely with the wind profile. Fig. 9 (e) also shows that operation in hyper-synchronous mode is assured and proved by the negative sign of the slip.

The direct rotor current varies close to a small value since it depends on the reactive power, as shown in Fig. 9 (f). The rotor quadrature current has the inverse form of the active power, as indicated in Fig. 9 (g).

During wind variation, the stator and rotor currents maintain a sinusoidal shape with a period of $0.02s$ as shown in Fig. 9 (i) and (j) respectively with a frequency equal to the mains frequency of $50Hz$.

The normalised THD value must be less than 5% for satisfactory power quality. In this study, the THD was less than 0.78%, as shown in Fig. 9 (h), indicating good power quality.

- **Robustness tests for Variable speed response**

The preceding test was conducted with the machine's characteristics fixed; nevertheless, these parameters are subject to a variety of physical phenomena, including temperature, which can cause resistance values to increase, inductor saturation, etc. Due to measurement tools and the used methodology, the identification of these factors is also stated in infidelities. To achieve this, the R_r and R_s values are increased by 50% compared with their nominal values. Fig. 10 shows the results obtained.

Fig. 10 shows that even if resistor and inductance value have changed, active and reactive power remain in line with reference values, and also remain decoupled. This shows that hybrid control by sliding mode backstepping is highly robust to parametric variations in the DFIG, due to good monitoring of power setpoints, with an almost identical response time on start-up.

8. Experimental validation

-Presentation of the experimental banc.

The hardware includes an FPGA Nexys3 board, a Semikron IGBT inverter, a Danfoss variable speed drive, a 1.5 KW squirrel cage induction machine (SCIM), a 1.5 KW DFIG, and a DSPACE 1104. Following the creation of the wind emulator, the inverter is used to apply the control algorithm to the DFIG rotor. The test bench summary is depicted in Fig. 12, and the actual realized test bench in the

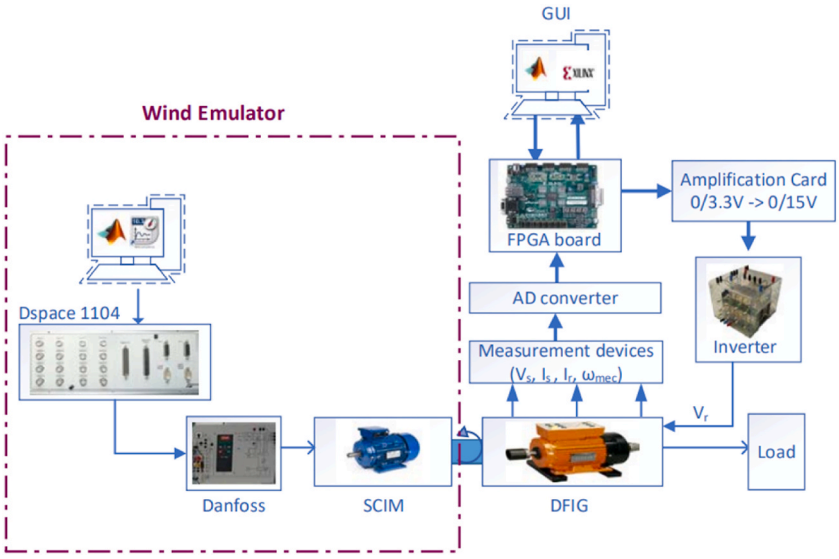

Fig. 12. Synopsis of the test bench.

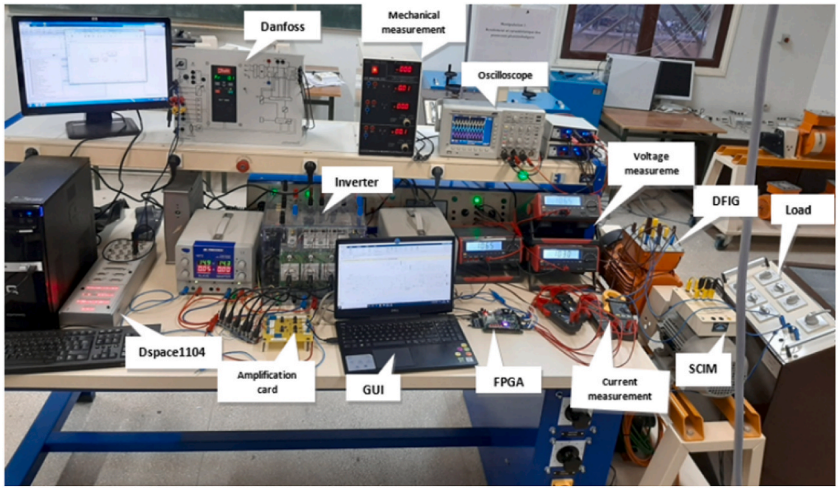

Fig. 13. Test bench.

laboratory is shown in Fig. 13.

- **Wind Emulator**

The DS1104 Board, as shown in Fig. 11 is used in the construction of the wind emulator. It's an interface board that can translate Simulink blocks into DSP-based system machine code. It comprises 8 ADC analog-to-digital converters with input voltages from −10 V to +10 V, and 8 DAC digital-to-analog converters with output voltages from −10 V to +10 V. It also features several interfaces, including digital inputs and outputs, incremental encoders, etc. The DS1104 board also features a slave DSP, the TMS320F240 DSP, which will be used to generate PWM signals.

The development of the control system using Simulink blocks, system simulation, and real-time model execution via the Ds1104 board are the first steps in the prototype process. Through the use of the Dspace1104 board and the Danfoss drive (variable speed drive), the emulator is implemented. Next, this drive instructs the DFIG and SCIM to work together to achieve a mechanical speed that matches the applied wind profile.

- **Stability analysis**

After modeling and simulating the hybrid sliding-mode backstepping control of a DFIG-based wind power system on Matlab/

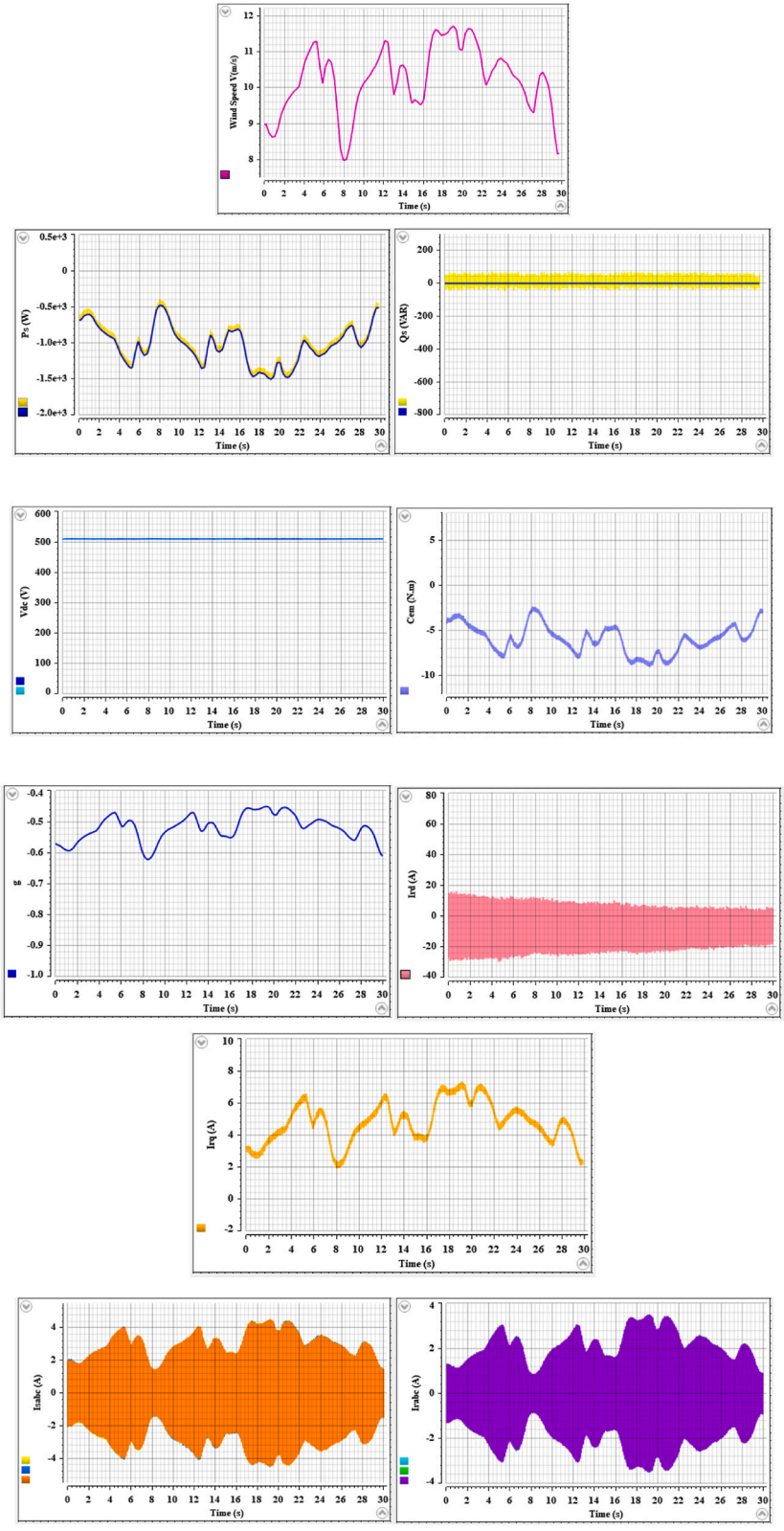

Fig. 14. DSPACE Control-Desk real time simulation results.

Table 2
Comparison between our proposed method and other controller technologies published recently.

Ref	Control method	Response Time (s)	Error (%)	THD (%)	Robustness
[65]	FOC	0.8	0.3184	–	Low
	Backstepping adaptive	0.1	1.47	–	
[42]	Sliding Mode	0.0858	–	3.99	Medium
	Backstepping	0.09	–	2.36	High
[35]	DPC based SM	–	–	5.56	Low
Proposed technique	Hybrid SM-BS	0.069	0.2	0.78	High

Simulink, real-time control is carried out using Al Hoceima region's profile and a computer connected to the Dspace DS1104 board with an RTI interface to Simulink through which they can convert Simulink blocks into machine code that can be run on a DSP-based system and also using ControlDesk that is used to display in real time the different variables of the program developed in Simulink. Next Generation 5.4 version 2.0.

The DS1104 Board, as shown in Fig. 11, comprises 8 ADC analog-to-digital converters with input voltages from −10 V to +10 V, and 8 DAC digital-to-analog converters with output voltages from −10 V to +10 V. It also features several interfaces, including digital inputs and outputs, incremental encoders, etc. The DS1104 board also features a slave DSP, the TMS320F240 DSP, which will be used to generate PWM signals.

ControlDesk is an interface that allows you to visualize in real time various variables in the program developed in Simulink, and also to modify parameters defining the operating mode of the blocks making up the Simulink diagram.

The experimental findings for a DFIG-based wind power system are shown in Fig. 14 after loading the sdf file on Control Desk from the Matlab/Simulink model at the RTI interface. This was done by applying hybrid sliding-mode Backstepping control to both the RSC and GSC converters. With regard to these findings, we observe improved grid power quality based on shape (sinusoidal with a frequency of 50 Hz) and decreased THD. In comparison to references, the active and reactive powers provide superior tracking. In terms of speed, THD accuracy, and robustness, the experimental findings are remarkably similar to the simulation results.

- **COMPARATIVE STUDY**

Table 2 presents a comparison study of the results between the control developed and another recent research. The reduction in response time for the first two controls [65], FOC and Adaptive Backstepping, is undoubtedly the main benefit of the hybrid SM-Backsteping control. It's also noteworthy that this study's THD was significantly lower than any of the five suggested control groups. In conclusion, in terms of performance, robustness, and quality, the SM-Backstepping hybrid controller provides the higher power generation.

9. Conclusion

The blending of sliding-mode and backstepping control has resulted in the hybrid control highlighted in this article. It used them to bring together the advantages of each and finally obtain a control that is efficient and robust against parametric variations. Starting with a study of all the elements in the conversion chain of the DFIG-based wind power system, followed by a clear insight into the principle of the sliding mode control law strategy and Backstepping, as well as the hybrid control mechanism and their applications to the two converters RSC and GSC.

Finally, accuracy and robustness against parametric variations are verified by simulation on Matlab/Simulink software and by real-time implementation on the DSPACE DS1104 board in a test bench. When compared to previous control systems, the SM-Backstepping hybrid controller has demonstrated significant potential in terms of quality and tracking reference since it has been able to eradicate the "CHATTERING" issue without compromising system performance. When compared to other current techniques, all of the results obtained in terms of tracking, robustness, and quality of electrical energy provided to the grid satisfy the needed performance criteria, indicating the effectiveness of the suggested controller. In the future, other hybridizations will be considered to achieve the desired performance in the case of an unbalanced grid.

CRediT authorship contribution statement

Farah Echiheb: Writing – original draft, Formal analysis, Data curation, Conceptualization. **Ismail Elkafazi:** Software, Methodology, Investigation. **Badre Bossoufi:** Validation, Supervision, Software. **Brahim El bhiri:** Visualization, Supervision, Project administration. **Mishari Metab Almalki:** Validation, Software, Resources. **Thamer A.H.Alghamdi:** Software, Resources, Project administration, Funding acquisition.

Declaration of competing interest

The authors declare the following financial interests/personal relationships which may be considered as potential competing interests:Badre BOSSOUFI reports financial support was provided by Sidi Mohamed Ben Abdellah University Faculty of Sciences Dhar El

Mahraz. Badre BOSSOUFI reports a relationship with Sidi Mohamed Ben Abdellah University Faculty of Sciences Dhar El Mahraz that includes: employment. If there are other authors, they declare that they have no known competing financial interests or personal relationships that could have appeared to influence the work reported in this paper.

References

[1] B. Pang, X. Zhu, J. Yang, K. Liao, B. Chen, Z. He, Voltage harmonics optimization for weak grid-tied doubly-fed induction generator with the capability of suppressing current harmonics, IEEE Trans. Energy Convers. (2023).
[2] K. Liao, B. Pang, J. Yang, Z. He, Output current quality improvement for VSC with capability of compensating voltage harmonics, IEEE Trans. Ind. Electron. (2023).
[3] K. Obaideen, M.N. AlMallahi, A.H. Alami, M. Ramadan, M.A. Abdelkareem, N. Shehata, A.G. Olabi, On the contribution of solar energy to sustainable developments goals: case study on Mohammed bin Rashid Al Maktoum Solar Park, International Journal of Thermofluids 12 (2021) 100123.
[4] Youssef Akarne, Ahmed Essadki, Tamou Nasser, et al., Modelling and control of a grid-connected AC microgrid with the integration of an electric vehicle, Clean Energy 7 (4) (2023) 707–720.
[5] M. Elgendi, M. AlMallahi, A. Abdelkhalig, M.Y. Selim, A review of wind turbines in complex terrain, International Journal of Thermofluids 100289 (2023).
[6] K. Zhang, B. Tang, L. Deng, X. Yu, J. Wei, Fault source location of wind turbine based on heterogeneous nodes complex network, Eng. Appl. Artif. Intell. 103 (2021) 104300.
[7] C. Jung, D. Schindler, Efficiency and effectiveness of global onshore wind energy utilization, Energy Convers. Manag. 280 (2023) 116788.
[8] A. Razmjoo, L.G. Kaigutha, M.V. Rad, M. Marzband, A. Davarpanah, M. Denai, A Technical analysis investigating energy sustainability utilizing reliable renewable energy sources to reduce CO2 emissions in a high potential area, Renew. Energy 164 (2021) 46–57.
[9] L. Sanderink, N. Nasiritousi, How institutional interactions can strengthen effectiveness: the case of multi-stakeholder partnerships for renewable energy, Energy Pol. 141 (2020) 111447.
[10] Y. Mourabit, A. Derouich, A. ElGhzizal, N. El Ouanjli, O. Zamzoum, Nonlinear backstepping control of variable speed wind turbine based on permanent magnet synchronous generator, in: Paper Presented at: International Conference on Wireless Technologies, Embedded and Intelligent Systems, WITS, IEEE, 2019, pp. 1–7.
[11] M. Yessef, H. Benbouhenni, M. Taoussi, A. Lagrioui, I. Colak, B. Bossoufi, T.A. Alghamdi, Experimental validation of feedback PI controllers for multi-rotor wind energy conversion systems, IEEE Access (2024).
[12] C. Hamid, D. Aziz, O. Zamzoum, A. El Idrissi, Robust control system for DFIG-based WECS and energy storage in reel wind conditions, EAI Endorsed Transactions on Energy Web 11 (2024).
[13] Factsheets on the European union. https://europarl.europa.eu/, 2023. (Accessed 10 January 2024).
[14] O. Apata, D.T.O. Oyedokun, An overview of control techniques for wind turbine systems, Scientific African 10 (2020) e00566.
[15] Z. Jiang, Installation of offshore wind turbines: a technical review, Renew. Sustain. Energy Rev. 139 (2021) 110576.
[16] D. Maradin, Advantages and disadvantages of renewable energy sources utilization, Int. J. Energy Econ. Pol. (2021).
[17] P. Sadorsky, Wind energy for sustainable development: driving factors and future outlook, J. Clean. Prod. 289 (2021) 125779.
[18] M.S. Nazir, N. Ali, M. Bilal, H.M. Iqbal, Potential environmental impacts of wind energy development: a global perspective, Current Opinion in Environmental Science & Health 13 (2020) 85–90.
[19] H. Benbouhenni, M.I. Mosaad, I. Colak, N. Bizon, H. Gasmi, M. Aljohani, E. Abdelkarim, Fractional-order synergetic control of the asynchronous generator-based variable-speed multi-rotor wind power systems, IEEE Access 11 (2023) 133490–133508.
[20] H. Benbouhenni, N. Bizon, I. Colak, M.I. Mosaad, M. Yessef, Direct active and reactive powers control of double-powered asynchronous generators in multi-rotor wind power systems using modified synergetic control, Energy Rep. 10 (2023) 4286–4301.
[21] H. Benbouhenni, N. Bizon, M.I. Mosaad, I. Colak, A. Djilali, H. Gasmi, Enhancement of the power quality of DFIG-based dual-rotor wind turbine systems using fractional order fuzzy controller, Expert Syst. Appl. (2023) 121695.
[22] X. Gao, Z. Wang, L. Ding, W. Bao, Z. Wang, Q. Hao, A novel virtual synchronous generator control scheme of DFIG-based wind turbine generators based on the rotor current-induced electromotive force, Int. J. Electr. Power Energy Syst. 156 (2024) 109688.
[23] C. Li, Y. Cao, B. Li, S. Wang, P. Chen, A novel power control scheme for distributed DFIG based on cooperation of hybrid energy storage system and grid-side converter, Int. J. Electr. Power Energy Syst. 157 (2024) 109801.
[24] S. Alshamali, D. Alawadhi, E. Aljuwaiser, Nonlinear control design for maximum power point tracking of a PMSG-based wind turbine, Int. J. Innov. Comput. Inf. Control 20 (2024) 313–328.
[25] N.E. Costa, G. Revel, D.M. Alonso, R.D. Fernández, Detection of the stability boundary associated to subsynchronous oscillations in DFIG based wind farms, Int. J. Electr. Power Energy Syst. 146 (2023) 108783.
[26] A.L. Miloudi Abderaouf, ETUDE DE LA COMMANDE INTRLLIGENTE D'UNE MACHINE ASYNCHRONE, Doctoral dissertation, faculté des sciences et de la technologie* univ bba), 2023.
[27] N. El Ouanjli, S. Motahhir, A. Derouich, A. El Ghzizal, A. Chebabhi, M. Taoussi, Improved DTC strategy of doubly fed induction motor using fuzzy logic controller, Energy Rep. (5) (2019) 271–279. Elsevier.
[28] Bo Yang, Tao Yu, Hongchun Shu, Jun Dong, Lin Jiang, Robust sliding-mode control of wind energy conversion systems for optimal power extraction via nonlinear perturbation observers, Appl. Energy 210 (2018) 711–723.
[29] G. Abdelhak, N. Abdellatif, D. Youcef, Backstepping control of a wind energy conversion systems based on a DFIG connected to the grid, Przeglad Elektrotechniczny 2023 (12) (2023).
[30] H. Benbouhenni, I. Colak, N. Bizon, A.G. Mazare, P. Thounthong, Direct vector control using feedback PI controllers of a DPAG supplied by a two-level PWM inverter for a multi-rotor wind turbine system, Arabian J. Sci. Eng. 48 (11) (2023) 15177–15193.
[31] A.J. Laafou, A.A. Madi, A. Addaim, Dynamic control of DFIG used in wind power production, based on PI regulator, in: 2020 IEEE 2nd International Conference on Electronics, Control, Optimization and Computer Science (ICECOCS), IEEE, 2020, December, pp. 1–6.
[32] B. Desalegn, D. Gebeyehu, B. Tamrat, Evaluating the performances of PI controller (2DOF) under linear and nonlinear operations of DFIG-based WECS: a simulation study, Heliyon 8 (12) (2022) e11912.
[33] M.S.H. Khan, S.K. Mallik, Mechanical sensorless control of a rotor-tied DFIG wind energy conversion system using a high gain observer, Journal of King Saud University-Engineering Sciences (2022).
[34] H. Chojaa, A. Derouich, O. Zamzoum, S. Mahfoud, M. Taoussi, H. Albalawi, M.I. Mosaad, A novel DPC approach for DFIG-based variable speed wind power systems using DSpace, IEEE Access 11 (2023) 9493–9510.
[35] H. Lhachimi, Y. Sayouti, Y. El Kouari, Optimal improvement of direct power control strategy based on sliding mode controllers, Comput. Electr. Eng. 71 (2018) 637–656.
[36] G. Nurettin, A. Sevinç, Performance study and analysis between vector control and direct power control for DFIG based wind energy system, International Journal of Energetica 6 (2021) 13–20.
[37] S.V. Savarkar, S.B. Singh, A comparison of performance of DPC technique for DFIG with using PI and PID controller, in: Advances in Renewable Energy and Sustainable Environment: Select Proceedings of NCRESE 2019, Springer Singapore, Singapore, 2020, pp. 117–129.
[38] H. Parivar, M. Shivaie, A. Darahi, M. Ansari, An efficient direct torque control strategy for a doubly fed induction generator (DFIG) in wind energy conversation systems, in: 2021 IEEE Texas Power and Energy Conference (TPEC), IEEE, 2021, February, pp. 1–5.
[39] H. Fethia, A. Amel, DTC-DPC of induction machine connected to wind generator, in: Artificial Intelligence and Renewables towards an Energy Transition, vol. 4, Springer International Publishing, 2021, pp. 79–87.

[40] A. Mirzakhani, R. Ghandehari, S.A. Davari, Performance improvement of DPC in DFIGs during unbalanced grid voltage based on extended power theory, Ain Shams Eng. J. 12 (2) (2021) 1775–1786.

[41] A.D. Falehi, An innovative optimal RPO-FOSMC based on multi-objective grasshopper optimization algorithm for DFIG-based wind turbine to augment MPPT and FRT capabilities, Chaos, Solit. Fractals 130 (2020) 109407.

[42] A.D. Falehi, H. Torkaman, Promoted supercapacitor control scheme based on robust fractional-order super-twisting sliding mode control for dynamic voltage restorer to enhance FRT and PQ capabilities of DFIG-based wind turbine, J. Energy Storage 42 (2021) 102983.

[43] A. Darvish Falehi, Optimal power tracking of DFIG-based wind turbine using MOGWO-based fractional-order sliding mode controller, J. Sol. Energy Eng. 142 (3) (2020) 031004.

[44] E.H. Bekkour, B. Bossoufi, A. Essalmi, H. El Alami, Design of a new and improved non-linear non-adaptive backstepping vector controller for a permanent magnet synchronous motor, in: International Conference on Digital Technologies and Applications, Springer International Publishing, Cham, 2022, January, pp. 524–534.

[45] F. Echiheb, Y. Ihedrane, B. Bossoufi, M. Bouderbala, S. Motahhir, M. Masud, S. Aljahdali, M. ElGhamrasni, Robust sliding-Backstepping mode control of a wind system based on the DFIG generator, Sci. Rep. 12 (1) (2022), https://doi.org/10.1038/s41598-022-15960-7.

[46] M.A. Soomro, Z.A. Memon, M. Kumar, M.H. Baloch, Wind energy integration: dynamic modeling and control of DFIG based on super twisting fractional order terminal sliding mode controller, Energy Rep. 7 (2021) 6031–6043.

[47] R. Hiremath, T. Moger, Modified Super Twisting algorithm based sliding mode control for LVRT enhancement of DFIG driven wind system, Energy Rep. 8 (2022) 3600–3613.

[48] Badre Bossoufi, Mohammed Karim, Mohammed Taoussi, Hala Alami Aroussi, Manale Bouderbala, Saad Motahhir, Mamadou Baïlo Camara'' DSPACE-based implementation for observer backstepping power control of DFIG wind turbine'', IET Electr. Power Appl. (2020) https://doi.org/10.1049/iet-epa.2020.0364.

[49] F. Echiheb, B. Bossoufi, I. El Kafazi, B. El Bhiri, A review backstepping control of a DFIG-based wind power system, in: International Conference on Digital Technologies and Applications, Springer Nature Switzerland, Cham, 2023, January, pp. 735–744.

[50] K. Liao, B. Pang, J. Yang, X. Jin, B. Chen, Z. He, Enhanced compensation strategy of voltage harmonics for doubly-fed induction generator, Int. J. Electr. Power Energy Syst. 148 (2023) 108924.

[51] B.S.V. Sai, R. Mohanty, S. Mohanty, D. Chatterjee, C. Dhanamjayulu, R. Chinthaginjala, A. Elrashidi, An efficient MPPT techniques for inter-harmonic reduction in grid connected hybrid wind and solar energy systems, Heliyon 10 (5) (2024) e27312.

[52] X. Zhang, J. Jia, L. Zheng, W. Yi, Z. Zhang, Maximum power point tracking algorithms for wind power generation system: review, comparison and analysis, Energy Sci. Eng. 11 (1) (2023) 430–444.

[53] R.A. Vilanculos, S. Mubiala, Etude et simulation de la commande vectorielle d'une MADA dédiée à un système aérogénérateur (Doctoral dissertation, Université Ibn Khaldoun Tiaret), 2022.

[54] E. Chetouani, Y. Errami, A. Obbadi, S. Sahnoun, Self-adapting PI controller for grid-connected DFIG wind turbines based on recurrent neural network optimization control under unbalanced grid faults, Elec. Power Syst. Res. 214 (2023) 108829.

[55] M.E. Azzaoui, H. Mahmoudi, Fuzzy-PI control of a doubly fed induction generator-based wind power system, Int. J. Autom. Control 11 (1) (2017) 54–66.

[56] R. Bendjaida, A.F. Benallal, Contrôle et Diagnostic des convertisseurs AC/DC à deux et trois niveaux dans une chaine éolienne basée sur une GSAP (Doctoral dissertation, Université Ibn Khaldoun), 2023.

[57] A. Hannachi, Etude et analyse de la modulation MLI et Hystérésis en vue de la commande des convertisseurs AC/DC/AC à deux et trois niveaux (Doctoral dissertation), 2022.

[58] W.T. Belharazem, I. Bendeddouche, Etude, Modélisation et commande robuste d'une éolienne (Doctoral dissertation, Directeur: Mr CHEMIDI Abdelkarim), 2023.

[59] D. Bezzina, Etude, modélisation et commande d'un système éolien à base d'une machine asynchrone à double alimentation connectée au réseau électrique (Doctoral dissertation), 2023.

[60] L. Saihi, Y. Bakou, A. Harrouz, I. Colak, K. Kayisli, R. Bayindir, A comparative study between robust control sliding mode and backstepping of a DFIG integrated to wind power system. 7th International Conference on Smart Grid, IcSmartGrid 2019, 2019, pp. 137–143, https://doi.org/10.1109/icSmartGrid48354.2019.8990810.

[61] Y. Mousavi, G. Bevan, I.B. Kucukdemiral, A. Fekih, Observer-based high-order sliding mode control of DFIG-based wind energy conversion systems subjected to sensor faults, IEEE Trans. Ind. Appl. (2023).

[62] Z. Bouguerra, Comparative study between PI, FLC, SMC and Fuzzy sliding mode controllers of DFIG wind turbine, Journal of Renewable Energies 26 (2) (2023) 209–223.

[63] M.A. Karami, S.M. Shariatmadar, M.E. Nazari, J. Rahmani-Fard, High-order sliding mode control of rotor-side converter in doubly-fed wind power generation system, Sci. Iran. (2023).

[64] D. Zellouma, H. Benbouhenni, Y. Bekakra, Backstepping control based on a third-order sliding mode controller to regulate the torque and flux of asynchronous motor drive, Periodica Polytechnica Electrical Engineering and Computer Science 67 (1) (2023) 10–20.

[65] M. Taoussi, M. Karim, D. Hammoumi, C. el Bekkali, B. Bossoufi, N. el Ouanjli, Comparative study between backstepping adaptive and field-oriented control of the DFIG applied to wind turbines. Proceedings - 3rd International Conference on Advanced Technologies for Signal and Image Processing, 2017, October 19, https://doi.org/10.1109/ATSIP.2017.8075592. ATSIP 2017.

[66] M. Atallah, A. Mezouar, K. Belgacem, M.A. Benmahdjoub, Y. Saidi, B. Brahmi, Grid synchronization of equivalent wind farm equipped with DFIG model for transient stability by using nonlinear integral backstepping control, Arabian J. Sci. Eng. 48 (5) (2023) 5771–5783.

[67] D. Zellouma, Y. Bekakra, H. Benbouhenni, Robust synergetic-sliding mode-based-backstepping control of induction motor with MRAS technique, Energy Rep. 10 (2023) 3665–3680.

[68] A. Kasbi, A. Rahali, MPPT performance and power quality improvement by using fractional-order adaptive backstepping control of a DFIG-based wind turbine with disturbance and uncertain parameters, Arabian J. Sci. Eng. 48 (5) (2023) 6595–6614.

[69] A. Eskandari, R. Vatankhah, E. Azadi, Optimization of wind energy extraction for variable speed wind turbines using fuzzy backstepping sliding mode control based on multi objective PSO, Ocean Eng. 285 (2023) 115378.

[70] Y. Ihedrane, C. El Bekkali, M. El Ghamrasni, S. Mensou, B. Bossoufi, Improved wind system using non-linear power control, Indonesian Journal of Electrical Engineering and Computer Science 14 (3) (2019) 1148–1158.

[71] O.S. Adekanle, M. Guisser, E. Abdelmounim, M. Aboulfatah, Observer-based adaptive backstepping control of grid-connected wind turbine under deep grid voltage dip, in: Hani S. El, M. Essaaidi (Eds.), Recent Advances in Electrical and Information Technologies for Sustainable Development, Advances in Science, Technology & Innovation (IEREK Interdisciplinary Series for Sustainable Development), Springer, Cham, 2019.

[72] Nadour Mohamed, Essadki Ahmed, Tamou Nasser, Comparative analysis between PI & Backstepping control strategies of DFIG driven by wind turbine, Int. J. Renew. Energy Resour. 7 (3) (2017).

[73] T. K Roy, M. A Mahmud, A.M.T. Oo, Nonlinear Backstepping Controller Design for Improving Fault Ride through Capabilities of DFIG-Based Wind Farms, 2018 IEEE Power & Energy Society General Meeting (PESGM), 2018.